J Eng Math (2009) 64:403–415
DOI 10.1007/s10665-009-9274-2

Coupled autoregulation models in the cerebro-vasculature

T. David · S. Alzaidi · H. Farr

Received: 31 May 2008 / Accepted: 4 February 2009 / Published online: 25 February 2009

Abstract A non-dimensional representation of both myogenic and metabolic autoregulation coupled with an asymmetric binary tree algorithm simulating the cerebro-vasculature has been developed. Results are presented for an autoregulation algorithm of the cerebro-vasculature downstream of the efferent arteries, in this case the middle cerebral artery. These results indicate that, due to the low pressures found in the arteriolar structure, the myogenic mechanism based on the increased open probability due to pressure of stretched activated ion channels does not provide enough variation in the vascular resistance to support constancy of blood flow to the cerebral tissue under variable perfusion pressure. A metabolic model has been developed under the assumption of close proximity between venules and the vascular tree at the arteriolar level. This allows carbon dioxide to diffuse between arterioles and the venous bed causing either a relaxation or contraction of the nearby arteriolar bed. Results show that the metabolic mechanism seems to be the dominant mechanism for cerebral autoregulation.

Keywords Autoregulation · Blood flow · Cerebro-vasculature · Differential equations

1 Introduction

Cerebral tissue requires a constancy of both oxygen and nutrients (notably glucose). During periods of pressure variation, which occur throughout the normal day as well as in cases of pathological hypo- and hyper-tension, the body's cerebral autoregulation mechanism cause the arterioles to vasoconstrict/dilate in response to changes in cerebral perfusion pressure over a certain range, thus maintaining a relatively constant cerebral blood flow. These effects are of particular importance when investigating how blood is redistributed not only via the circle of Willis but throughout the cerebral tissue. It should be noted that there have been a number of cerebral autoregulation models proposed [1–3], including models incorporated with a circle of Willis [4–11]. However, the combination of an autoregulation model with a fully populated arterial tree able to regulate dynamically remains a relatively unexplored field.

Considerable research effort has been expended in furthering the understanding of how an artery alters its radius and the associated chemical pathways. Particular interest has focused on the myogenic mechanism where the systemic blood pressure exerts an influence on vascular smooth muscle, an excellent review can be found in [12].

T. David (✉) · S. Alzaidi · H. Farr
Center for Bioengineering, University of Canterbury, Christchurch, New Zealand
e-mail: tim.david@canterbury.ac.nz

Fundamental studies were carried out by Harder [13,14] and Harder et al. [15]. Less research has been done for the metabolic condition where variations in pH and CO_2 are considered to be the prime movers for dilation/contraction of the small arterioles deep in the vascular tree. The most comprehensive study of blood flow control has been that of [16], however even in this case several important constants remain unknown making the model somewhat constrained.

The present model uses previous work by Gonzalez–Ferrandez and Ermentrout [17] to closely couple a myogenic model and a new metabolic model of cerebral autoregulation with a representation of a vascular tree taken from the work of [18]. In order to allow all parts of the tree to vary in its arterial radius (and hence resistance) the myogenic and metabolic models are non-dimensionalised enabling a single algorithm to be utilised. The work shows that in order to replicate the well-known variation of peripheral resistance with pressure the metabolic model is by far the dominant mechanism, so much so that the myogenic mechanism seems to hardly play a role.

2 Theory and methodology

The models for both myogenic and metabolic autoregulation were constructed with the aim of simplicity in formulation as much as possible while still upholding the correct experimentally observed observations. The myogenic model is based on the original work of Gonzalez–Ferrandez and Ermentrout [17] here termed the GFE model. This work modelled the experimental evidence of Harder [13,14] which investigated the motion of cat cerebral arteries. Essentially the GFE model utilises differential equations to simulate Ca^{2+} variations in smooth muscle via Ca^{2+} and Ca^{2+}-dependent K^+ ion channel open probabilities. The time-dependent calcium concentration variations are used to determine the variation in cross-bridge links to myocin light chain kinase and the subsequent contraction/dilation of the arterial wall. The wall is assumed to be made from a circumferential Maxwell unit where the parallel unit is a contractile one based on calcium concentration. In the interests of brevity we give only those equations which substantially differ (in their non-dimensional form) from that of the GFE model. Complete details of the original model and its assumptions can be found in [17].

2.1 The myogenic response

A vessel's transmural pressure determines a hoop stress, and via stress activated Ca^{2+} ion channels changes the calcium flux across a smooth muscle cell membrane. The resultant hoop, muscle and elastic stresses determine a rate of change of the vessel's diameter; this is the myogenic response. These changes are facilitated by electromechanical coupling within smooth muscle cells.

The myogenic response for a system of small arteries of the brain modelling an arterial bed can be represented by the system of dimensionless differential equations using the formulation and reasoning of the GFE model.

We choose characteristic values for the major variables in the model, such that

$$v_i = \frac{v'}{v_{\mathrm{Ca}}}, \quad T = \frac{t g_{\mathrm{Ca}}}{C}, \quad \left[\mathrm{Ca}^{2+}\right] = \frac{\left[\mathrm{Ca}^{2+'}\right]}{\alpha v_{\mathrm{Ca}} C}, \quad p = \frac{p'}{p_0}, \quad R = \frac{r_i}{r_0}, \tag{1}$$

where r_i, r_0 are the internal and external radii of an artery, p_0 is a reference pressure (nominally 100 mmHg), v' is the membrane potential, v_{Ca} the Nernst potential for the Ca^{2+} ion channel, g_{Ca} the Ca^{2+} ion channel conductance, C the cell capacitance, $[Ca^{2+'}]$ the cytosolic Ca^{2+} concentration and α represents the percentage charge contained in the cell volume.

The ion channel model is represented by both the Ca^{2+} channel and the Ca^{2+} mediated K^+ ion channels. The Ca^{2+} channel is assumed in equilibrium and therefore has the normal sigmoidal functional representation.

$$m_\infty = \frac{1}{2}\left[1 + \tanh\left(\frac{v - v_1}{v_2}\right)\right]. \tag{2}$$

In order to model the stretch activation of the Ca^{2+} channel the constant v_1 is varied using the same functional form as that found in the GFE model (a simple linear monotonic decreasing function of voltage with respect to pressure). The Ca^{2+} mediated K^+ channel has a slower reaction time so is written as a differential equation thus

$$\frac{dn}{dT} = \lambda_n (n_\infty - n), \quad n_\infty = \frac{1}{2}\left[1 + \tanh\left(\frac{v - v_3}{v_4}\right)\right], \quad \lambda_n = \phi_n \cosh\left(\frac{v - v_3}{2v_4}\right) \tag{3}$$

with

$$v_3 = -\frac{v_5}{2}\tanh\left(\frac{Ca_i - Ca_3}{Ca_4}\right) + v_6, \tag{4}$$

where Ca_3, Ca_4, v_1, v_2, v_3, v_4, v_5, v_6 are all known constants and appropriately non-dimensioned from the GFE model. The product of the time-rate of change of the membrane potential and the cell capacitance is balanced by the sum of the currents across the membrane, where g_j is the conductance of channel j and v_L a Nernst potential for the cell leakage.

$$C\frac{dv}{dT} = -\left[g_L (v - v_L) + g_K n (v - v_K) + m_\infty (v - 1)\right]. \tag{5}$$

The non-dimensional time rate of change of cytosolic calcium is given as

$$\frac{dCa_i}{dT} = -\rho\left[m_\infty (v - 1) - k_{Ca} Ca_i\right] + \gamma F(\tau_w) \tag{6}$$

with ρ the non-dimensional equivalent of that given in the GFE model and F, a function of the wall shear stress τ_w acting on the membrane of the endothelial cell is taken from the work by Wiesner et al. [19], determined from assuming that the shear-dependent influx to be proportional to the fraction of open Ca^{2+} channels (which has a Boltzmann dependence on the strain-energy density in the membrane). γ is used to determine the ratio of influx between the direct Ca^{2+} channel and that mediated by an Akt pathway (see (9), full details may be found in [20].

$$F(\tau_w) = \frac{1}{1 + \alpha \exp(-W(\tau_w))}, \quad W(\tau_w) = W_0 \frac{\left(\tau_w + \sqrt{16\delta^2 + \tau_w^2} - 4\delta\right)^2}{\tau_w + \sqrt{16\delta^2 + \tau_w^2}}. \tag{7}$$

Finally in this particular section we look at the rate of change of myocin–actin cross-bridge filaments. the resulting stress in the arterial wall depends on the number of cross-bridges formed between myosin and actin filaments. For a given myosin–actin overlapping segment, there is a maximum possible number of cross-bridges; let ω stand for the fraction of actual cross-bridges then the non-dimensional time rate of change of cross-bridge ratio becomes

$$\frac{d\omega}{dT} = k_\psi\left(\frac{\psi}{\psi_{ref} + \psi} - \omega\right), \quad \psi = \frac{Ca_i^3}{\left(Ca_{i,ref}\right)^3 + Ca_i^3} \tag{8}$$

with ψ representing the phosphorylation of the myocin light chain kinase and k_ψ a function of eNOS concentration as outlined below.

2.2 Endothelial nitric oxide synthase (eNOS) dynamics

Experiment has shown that arterial regions with low wall shear stress correspond with regions of impaired eNOS signalling in endothelial cells (cells lining the lumen of blood vessels) and hence the reduced availability of NO, a potent vasodilator. It is believed that while heightened blood pressure causes arterial smooth muscle to contract, higher wall shear stress acts as a counterbalance to this response, causing arterial walls to dilate.

The dynamics of eNOS and how they change as a function of wall shear stress is given by Comerford et al. [20]. The non-dimensioned version of the differential equation governing the conservation of eNOS is given by

$$\frac{d}{dT}\text{eNOS} = \frac{k_{dis} Ca_i}{Ca_i + \kappa} - \mu\ \text{eNOS} + (1-\gamma)\, g_{max} F(\tau_w). \tag{9}$$

Here the first term on the right-hand-side models the production of eNOS through a calcium-dependent pathway, the second a simple decay rate and the third through a calcium-independent Akt pathway [21] which is a function of wall shear stress.

Note: While the GFE model simulates the dynamics of species within smooth muscle cells, that of Comerford et al. [20] models the dynamics within endothelial cells. For simplicity, it is assumed that any change in concentration of a chemical species in the endothelial cell is instantaneously propagated to the smooth muscle cell and vice versa.

The experiments of van Riper et al. [22] involve the injection of artificial nitrovasodilators such as nitroglycerin into histamine-contracted arterial smooth muscle. Their results show that nitrovasodilators cause significant decreases in phosphorylation without significant changes in intracellular calcium, suggesting that nitrovasodilators decrease calcium sensitivity of MLC phosphorylation. In the light of this the following changes to the differential equation (cross-bridge fraction) for the myosin cross-bridges above were thus made.

$$\frac{\mathrm{d}\omega}{\mathrm{d}T} = k_{\mathrm{eNOS}} \left(\frac{\psi}{\psi_{\mathrm{ref}} + \psi} - \omega \right), \tag{10}$$

where

$$k_{\mathrm{eNOS}} = 1 - \beta\,[\mathrm{eNOS}]. \tag{11}$$

Here k_{eNOS} expresses a decrease in phosphorylation with increasing eNOS concentration, where $\beta = 10^6$ is a constant found from experimental data, assuming a linear relationship between nitrovasodilator concentration and MLC phosphorylation. It has been assumed that eNOS (a natural nitrovasodilator) is a more effective vasodilator (releases NO more readily) than its artificial experimental counterpart, nitroglycerin, at cell conditions. Thus the experimental trend found from the van Riper data was altered by a factor of 20, thus expressing the relative increase in vasodilatory effectiveness by having eNOS as a vasodilator instead of nitroglycerin. It should be noted that varying β did not alter the myogenic response to any great degree.

Finally the process of non-dimensionalisation did not produce parameters small enough to be neglected nor reaction rates which could be considered to be in equilibrium.

2.3 Arterial-wall model

The GFE model utilises a combination of parallel, x (denoting the circumferential distance of the artery wall), and series u- and y-components to simulate the complete motion of the arterial wall, essentially a Maxwell unit. The y-unit is contractile and dependent on the amount of cross-bridges (and hence Ca^{2+}) whilst that of u and x are purely elastic. The rate of change of circumferential distance (essential the radial width of the artery) is given by the sum of forces acting on the Maxwell unit. These are due to the non-dimensional systemic blood pressure $f_{\Delta p}$, the restoring force due to the two elastic components f_x and f_u. In its non-dimensional form the time rate of change of the arterial circumference x is given by

$$\frac{\mathrm{d}x}{\mathrm{d}T} = \frac{1}{\zeta} \left(f_{\Delta p} - f_x - f_u \right) \tag{12}$$

with

$$\frac{1}{\zeta} = \frac{0.8\sigma_0^{\#} C}{\tau g_{\mathrm{Ca}} \pi} \frac{(1-R)}{(1+R)}, \tag{13}$$

where $\sigma_0^{\#}$ is the hoop stress corresponding to maximum muscle activation [23] and τ a characteristic time for smooth muscle cell relaxation. The rate of change of the contractile element length y is given by

$$\frac{\mathrm{d}y}{\mathrm{d}T} = \begin{cases} -v_{\mathrm{ref}} \frac{\psi}{\psi_{\mathrm{ref}}} a \frac{1 - \frac{\sigma_u}{\sigma_y}}{a + \frac{\sigma_u}{\sigma_y}}; & \frac{\sigma_u}{\sigma_y} \in [0, 1] \\ c \left[\exp\left(b \left(\frac{\sigma_u}{\sigma_y} - d \right) \right) - \exp\left(b\,(1-d) \right) \right]; & \frac{\sigma_u}{\sigma_y} \in [1, \infty), \end{cases} \tag{14}$$

where $\sigma_y(\omega, y)$ and $\sigma_u(u)$ are the stresses due to the contractile element and the in-line elastic element which are functions of the number of phosphorylated chains ω and the elastic in-line element length, u, respectively [23, pp. 102–104]. ν_{ref}, a, b, c and are constants and ψ is as defined in (8). The hoop-stress force due to pressure Δp is given by

$$f_{\Delta p} = \frac{1}{2}\Delta p \frac{(1+R)}{(1-R)}\left[\frac{x}{0.8} - \frac{0.8}{x}\frac{(1-R)}{(1+R)}\right] \tag{15}$$

and for this particular model we use $R = 0.6$ [24]; f_x and f_u are the same as that given in the GFE model. The equation for u is a simple conservation of length $x = y + u$. Thus, the seven equations given by (3),(5),(6),(10),(9),(12) and (14) form a closed system which determines the circumference of the arterial radius for the myogenic mechanism.

2.4 Metabolic model

Although selective ion channels in the smooth muscle cell of the cerebro-vasculature respond to variations in both CO_2 and pH [25, Chap. 4, pp. 326–330] our initial model for the metabolic response uses the simple assumption that the set of arterioles feeding the capillary bed are in close proximity to the venous return. Excess carbon dioxide in the venules is diffused to the arterioles and induces a relaxation/contraction of the arteriolar radius thus allowing increased/decreased blood flow to convect away carbon dioxide and hence maintain the correct CO_2 concentration. This is similar to the work of [26] and has been used to partially explain the oscillations of oxygen cycles in cerebral flow [27]. This model was also used in the 1D models of [28]. Equation 16 represents a conservation equation where the rate of change of carbon dioxide is balanced by the production (due to metabolism) and that convected away by the blood flow.

$$\frac{\mathrm{d}CO_{2,\text{tissue}}}{\mathrm{d}t} = \text{CMRO}_2 + \text{CBF}\left(CO_{2,\text{artery}} - CO_{2,\text{tissue}}\right) \tag{16}$$

where $CO_{2,\text{tissue}}$ is the tissue concentration of carbon dioxide, $CO_{2,\text{artery}}$ is the arterial concentration of carbon dioxide (assumed to be 0.49 ml/ml) CMRO_2 is the cerebral metabolic rate of oxygen consumption (assumed to be a constant 0.035 ml/g/min for all parts of the brain), which due to the stoichiometry of the aerobic metabolism in the brain tissue, is equal to the cerebral metabolic rate of carbon dioxide production. CBF is the flow rate in the terminal artery and thus entering the capillary bed. We use a reverting differential equation for the radius of the arteriole given by

$$\frac{\mathrm{d}r}{\mathrm{d}t} = \frac{1}{\mu}\left(CO_{2,\text{sp}} - CO_{2,\text{tissue}}\right), \tag{17}$$

where $CO_{2,\text{sp}}$ is the steady-state solution to (16) and μ a characteristic time for the arterial smooth muscle cells to react. We choose the following non-dimensionalisation

$$c = \frac{CO_{2,\text{tissue}}}{CO_{2,\text{artery}}};\ t = \frac{T}{\text{CBF}_0};\ \chi = \frac{r}{r_0}, \tag{18}$$

where r_0 is the arterial radius and CBF_0 is the value of the blood flow in the terminating arteriole at normal physiological conditions (known quantities). With the above Eqs. 16 and 17 become

$$\frac{\mathrm{d}c}{\mathrm{d}T} = (\varepsilon - 1) + Q(1 - c) \tag{19}$$

and

$$\frac{\mathrm{d}\chi}{\mathrm{d}T} = -\xi(\varepsilon - c) \tag{20}$$

with

$$Q = \frac{\text{CBF}}{\text{CBF}_0};\ \varepsilon = 1 + \frac{\text{CMRO}_2}{CO_{2,\text{artery}}\text{CBF}_0} \tag{21}$$

and

$$\xi = \frac{CO_{2,\text{artery}}}{\mu r_0 \text{CBF}_0}. \tag{22}$$

2.5 Asymmetric binary tree model

The tree-branching algorithm used is that developed for the abdominal fractal vascular network of Olufsen et al. [18] and is based on two variables: a power exponent k (describing the relationship between parent vessel radius r_p and daughter vessels radii r_{d1} and r_{d2}, and an asymmetry ratio γ (describing the relative ratio between two daughter vessels). For this particular study a binary tree emulates the vascular system stemming from a major artery, say the middle cerebral artery (MCA) for example. The values of k and γ change depending on the location of the vessel in the tree, i.e., values are different for arteries, arterioles and capillaries. The length and radius of a vessel are related by a length to radius ratio (denoted l_{rr}, chosen as 20 for this model). Here we take values of k and γ as those given in [18]. Figure 1 shows a sketch of the basic network. The arterial tree code creates branching levels. At each branching level, two daughter vessels are created for each artery in the previous branching level. This process is repeated until all terminals reach the size of a pre-capillary sphincter (10μm). Each of these terminals is assumed to supply a bed of capillaries, all with 2.5μm radius.

The model has the ability to emulate actual vascular networks by using the statistical data of Lauwers et al. [29](data of radii and length of all vessels in a small section of the cortex). The mean and the standard deviation from this data population is implemented into the code so that each arterial segment in the tree has a probability density function that emulates this physiological data.

2.5.1 Peripheral resistance and pressure distribution evaluation

To find each individual resistance of each segment in the tree, the algorithm uses a Poiseuille-flow assumption such that the resistance of an arterial segment is proportional to the inverse of the fourth power of the radius. The viscosity is calculated using the diameter dependent equations from Pries and Secomb [30]. In order to find the flow and pressure distribution throughout the tree a single pass up and down the tree is required. Starting at each terminal segment a total resistance is evaluated for the two daughters and the parent artery assuming that the terminal segments are connected via the venous bed (essentially daughters in parallel with the parent in series). This parallel/series calculation is then done at each bifurcation of the tree until there is a single value of resistance. The total flow into the arterial tree is known and hence the total pressure drop can be evaluated. Moving down the tree the pressure drop and flow rate at and through each arterial segment is calculated respectively.

Figure 2 shows a pressure distribution as a function of all branching levels in the tree. Here the dots denote an average value whilst the bars indicate a single standard deviation limit. The tree consists of approximately 1,000,000

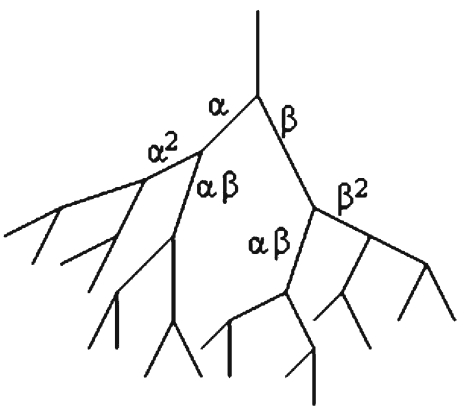

Fig. 1 A sketch of the asymmetric binary tree

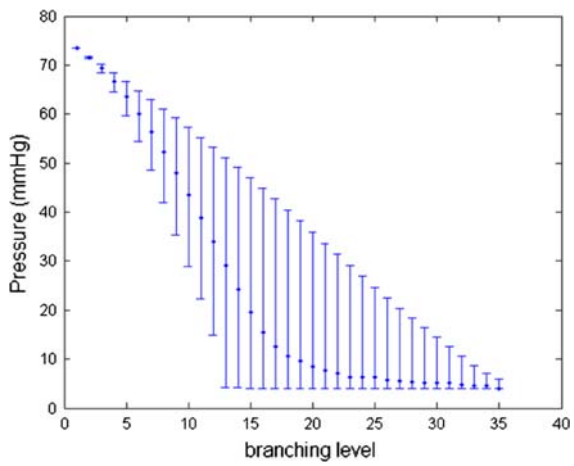

Fig. 2 Branching levels vs. pressure

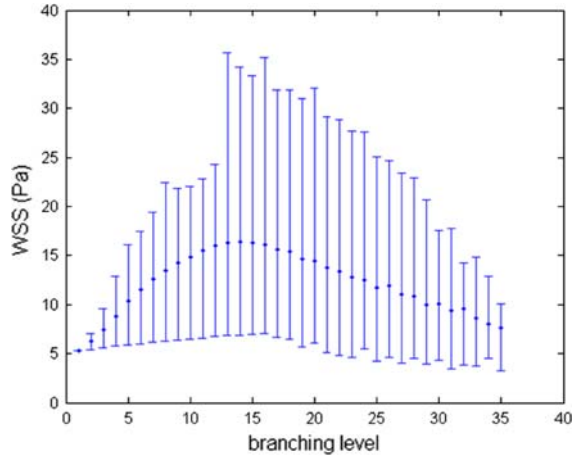

Fig. 3 Wall shear stress at each branching level

segments of which 500,000 are terminal segments. The blood pressure at the inlet to the MCA (Pa) and the venous pressure (Pv) at the end of the tree are both inputs.

The wall shear stress values that were calculated for each branching level of the arterial tree are shown in Fig. 3. The points represent the average value of wall shear stress, and the top and bottom bars give the maximum and minimum values of wall shear stress found at the same branching level.

Figure 4 indicates the cumulative peripheral resistance of the arterial bed as a function of branching level. The majority of resistance is obtained at approximately branch level 25. The tree is extended to a larger branch level in order to ensure that all terminal conditions are reached, even though it is not normally the case that anatomically a branch level of that greater than 25 can be found.

It is important to investigate the pressure distribution at the terminal arterioles since this provides information on the blood flow into the capillary bed. Figure 5 shows the pressure distribution as a function of branching level and indicates that terminal arterioles are not obtained until branch level 14. In addition the mean pressure at this level is only 13 mmHg with a maximum of nearly 18 mmHg as the branch levels increase the pressure decreases

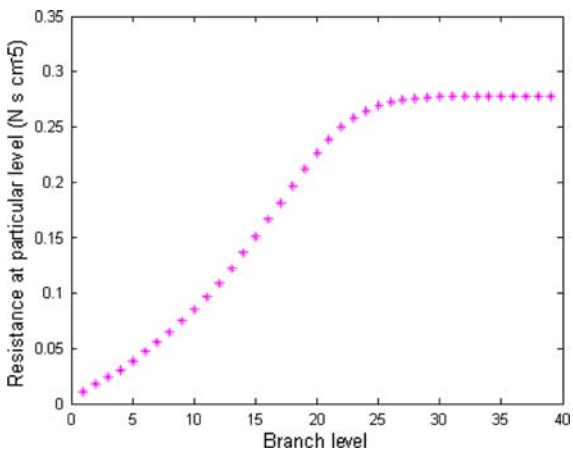

Fig. 4 Branching vs. cumulative resistance

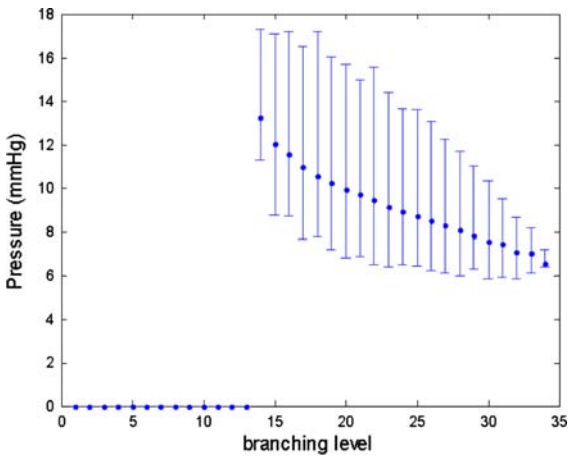

Fig. 5 The pressure distribution at terminal leaves as a function of branching level, (dots represent average values lines indicate standard deviation limits)

to a minimum of about 7 mmHg. These values will become important in comparing the relative responses between myogenic and metabolic mechanisms.

Finally Fig. 6 shows the number distribution of terminal arterioles as a function of pressure and indicates a skewed normal distribution correlating well with the data of Lauwers et al. [29].

2.5.2 Capillary bed

At each terminal segment the capillary bed consists of approximately 6,000 capillaries in parallel, each of which is modelled as an identical Krogh cylinder [31], and as analysed by Bloch [32], and Blum [33]. The number of capillaries is determined by the known perfused volume of brain tissue for that particular major efferent artery. Although both Bloch and Blum provided analytical solutions (for the steady-state condition) of oxygen consumption in a capillary the algorithm used in this simulation for evaluating the oxygen and carbon dioxide concentration within the cylinder is that given by McGuire and Secomb [34], details of which need not be given here.

2.5.3 Numerical methods

The differential Eqs. (3),(5),(6),(10),(9),(12) and (14) were solved using MATLAB's `ode23s` routine (based on a modified Rosenbrock formula of order 2 [35]) at zero pressure. The initial conditions at zero pressure for the set of differential equations were found using the equilibrium condition of the differential equations. The solution found at zero pressure is used as the initial conditions for the next pressure step. This process is then repeated at each pressure step. The solution at the final pressure is used as the initial condition for the pressure step before it, and this process completed in the opposite direction. The values found at each pressure in both directions are averaged. This is to ensure that any slightly erroneous initial conditions are corrected so as to give the most accurate values.

Despite the fact that transmural pressure and wall shear stress are coupled, they are treated as being independent for the purpose of simplicity of solution. Therefore, to calculate the response of an artery to wall shear stress and pressure, the pressure increment method described above is used assuming that wall shear stress is kept constant at each pressure step.

Values of the non-dimensional radius once they have reached an asymptotic value are stored in a data set of radius, wall shear stress and pressure creating a "look-up table". In order to change each arterial radius in the entire tree a bilinear interpolation method is used such that with a given wall shear stress and pressure the new radius of each artery is found in conjunction with the cerebral arterial tree model.

For the autoregulation model which uses only the metabolic model to change arterial radii, Eqs. 19 and 20 are solved to produce a look-up table consisting of non-dimensional radii versus pressure evaluated, as in the case of the myogenic model, at some large time where the radius has reached an asymptotic value.

2.5.4 Solution of autoregulation model with the asymmetric binary tree

All initial flow rates, pressure drops, and radii of all tree segments are calculated at the creation of the arterial tree as described above and using a known value of the initial radius (in this case the middle cerebral artery (1 mm) and a systemic pressure of 75 mmHg. This pressure value is derived from the 3D computational model of [4] to take into account the pressure drop through the circle of Willis. The WSS value and the pressure are used with the "look-up table" to find the corresponding radius value for each segment. All pressures and flow rates are then recalculated throughout the arterial tree with these new radii values by traversing up and down the tree to evaluate new pressures and flow rates. This process is then repeated until a simple convergence criterion on the total peripheral resistance is met.

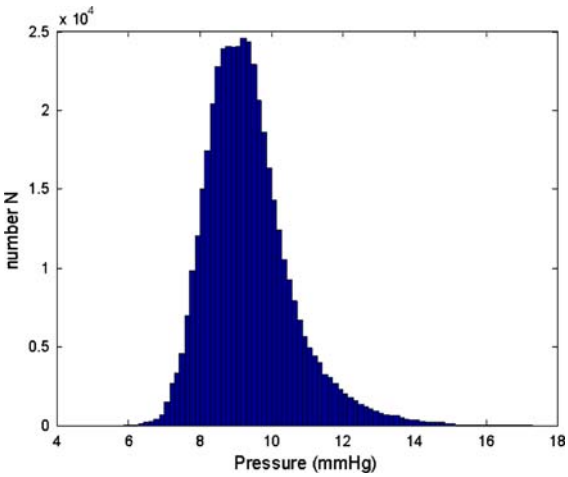

Fig. 6 Pressure vs. terminal distribution

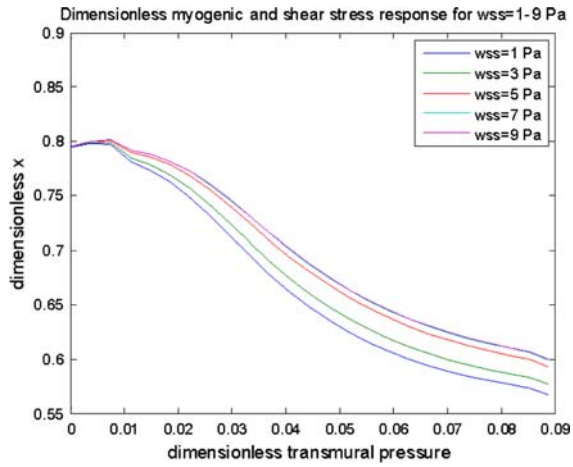

Fig. 7 Dimensionless pressure vs. dimensionless artery circumference, x, for WSS = 1–9

3 Results and discussion

3.1 Autoregulation model

3.1.1 Myogenic

The dimensionless myogenic response (for a single artery) including the effect of wall shear stress is shown in Fig. 7 for the range of physiological wall shear stress values (WSS 1–9 Pa).

The presented non-dimensional model correlates well with that of the GFE model results achieving first passive dilation, followed by active contraction of the arterial wall with increasing pressure ([17, Fig. 8]). The model also correctly simulates oscillations in the Ca^{2+} concentration resulting in vasomotion (results not shown). As expected these oscillations are absent for very low pressures.

We have assumed that all arteries in the arterial-tree model have approximately the same radius ratio R. This provides an important simplification, as it ensures that the dimensionless myogenic response is the same for any artery, which reduces computation. However, in reality, larger arteries have a relatively thicker wall than smaller arterioles due to larger amounts of elastic tissue and smooth muscle. Therefore, larger arteries have a larger R-value than smaller arterioles, a difference that could be later implemented into the arterial tree model.

The sigmoidal function $F(\tau_w)$ (see Eq. 7) determines to a certain extent the change in eNOS, and hence the change in vessel diameter due to wall shear stress. Due to this particular functional form the corresponding response due to wall shear stress is effectively bounded between two responses, i.e., effectively mimicking the sigmoidal function. Thus, the response with varying wall shear stress changes between approximately 1 and 8 Pa but is effectively unchanged at lower or higher values of wall shear stress. This potentially presents a problem in the solution of the arterial tree model using the autoregulation model; as one would expect very high or very low wall shear-stress values to make considerable difference to the response of an artery; however, this autoregulation model does not show this.

The value of β in the k_{eNOS} equation above (see Eq. 11) is an assumption and further experimental work is required to validate this value. It is also possible that a nonlinear function would better model the change in phosphorylation due to eNOS concentration.

The experiments of Lipowsky et al. [36] estimate arteriole wall shear stress values of approximately 5 Pa average, with a maximum value of 20 Pa. However, Fig. 3 gives the distribution of wall shear stress through the arterial tree

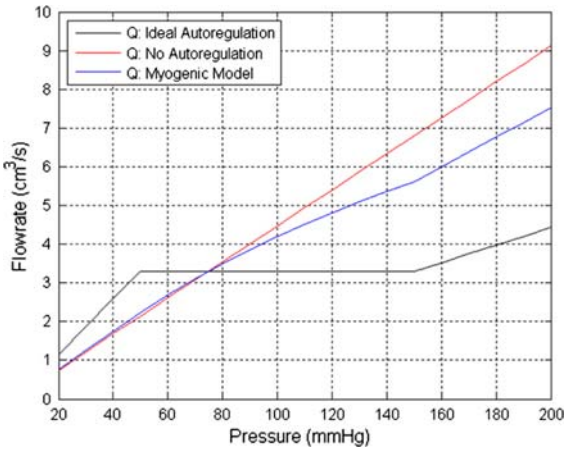

Fig. 8 Pressure vs. cerebral blood flowrate

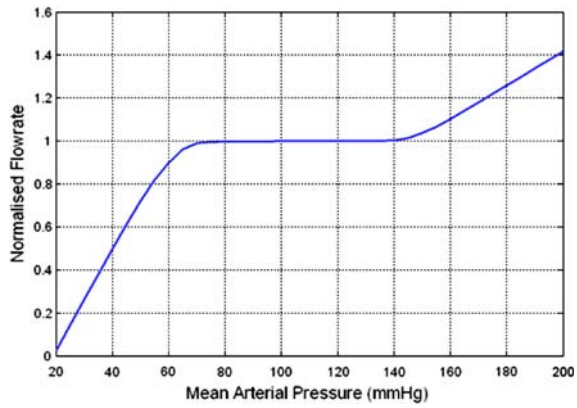

Fig. 9 Pressure vs. cerebral blood flowrate

with a range of wall shear stress values up to 40 Pa. At higher blood pressures, the maximum wall shear stress can reach 80 Pa. As a check average pressure gradient per unit length profiles were evaluated as a function of average arteriolar radius. These data compared very well with data from [36] (results not shown). Lipowsky's data suggests different correlations for wall shear stress are used for arteries with different diameters, as opposed to using the same equation for all vessels. It is possible that using these correlations with the arterial-tree model may produce wall shear-stress values within the expected physiological range. This is yet to be trialled.

Figure 8 plots for a range of systemic pressure the flowrate in the entire tree. This is a representation of the blood flow required to perfuse the brain tissue supported by the middle cerebral artery. The plot shows that although the myogenic autoregulation model does provide some change from the no autoregulation case, it does not successfully emulate the ideal observed autoregulatory response. For comparison, the no-autoregulation case and the ideal autoregulation response are also shown.

Figure 4 demonstrates that the smaller arterioles of this arterial tree contribute the vast majority of the total resistance of the tree, as expected. These smaller arterioles have very low pressures, and according to the myogenic autoregulation model only very small changes occur at these low pressures, indeed these changes could well be dilatory! In particular the low pressures at the arteriolar level mean that the constant υ_1 modeling variation in the stress activated Ca^{2+} channel defined in (2) does not change significantly. Consequently the equilibrium open probability for the Ca^{2+} channel does not change in response. When υ_1 remains at the zero pressure value then as shown in ([17, Fig. 9]) and replicated by our model, the vessel simply dilates as a function of increasing pressure. In addition changes in the vessel radius ratio R are relatively small when measured throughout the arterial tree, hence varying this value in (13) will not produce changes likely to provide the autoregulatory changes needed in response to changes in systemic pressure. Indeed the percentage change of the smaller arterioles (in the range of 10 and 100 μm) that is required to reach the ideal autoregulation profile is of the order of 30%. This change cannot be induced using the current myogenic autoregulation model at such low pressures found at the arteriolar level.

3.1.2 Metabolic

It has been experimentally shown by Lipowsky et al. [36] that the large collection of small arterioles makes up the majority of the resistance of an arterial tree. It is shown above that the current myogenic autoregulation model does not provide enough radial change in these smaller arterioles to facilitate the ideal autoregulation profile as shown in Fig. 8. The metabolic algorithm described above is now substituted for the myogenic model where the look-up table contains values of radius and pressure evaluated as before for large times so as to reach asymptotically stable values. For each pressure value ranging from 0 to 200 mmHg and for each pressure value in the tree the radii of

segments, where these radii lie between 10 and 100 μm, are changed in an iterative manner (using the look-up table previously evaluated from Eqs. 16 and 17 until a converged value of the total peripheral resistance is found. Segments of the tree with radii outside of the range given above are unchanged. This algorithm has been used to yield the following results. Figure 9 plots physiological perfusion pressure vs. the total normalised flow rate in the tree. This flow rate is normalised to that known value (2.85 mls^{-1} required to perfuse the volume of the brain supported by the middle cerebral artery at "normal" physiological conditions (systemic pressure of 100 mmHg). As can be seen the metabolic autoregulation model provides the correct variation in peripheral resistance to ensure constancy of flow rate to the cerebral tissue without myogenic support.

4 Conclusion

By developing a non-dimensional representation of the arterial wall model of Gonzalez–Ferrandez and Ermentrout [17] and the asymmetric binary tree algorithm of Olufsen et al. [18] results are presented for an autoregulation algorithm of the cerebro-vasculature downstream of the efferent arteries, in this case the middle cerebral artery. These results indicate that due to the low pressures found in the arteriolar structure the myogenic mechanism based on the increased open probability of stretched activated ion channels does not provide enough variation in the vascular resistance to support constancy of blood flow to the cerebral tissue under variable perfusion pressure. This particular outcome of the model is interesting since it highlights some of the difficulties for experimentalists in determining the correct (i.e., physiological) conditions when investigating the cellular mechanisms related to autoregulation of the vasculature. Indeed, it is important to note the gradient of fluid pressure as a function of "depth" in the vascular tree in conjunction with the use of Poiseuille's equation relating inversely the peripheral resistance to the fourth power of the vessel radius.

A relatively simple metabolic model has been developed under the assumption of close proximity between venules and the vascular tree at the arteriolar level (this close proximity is certainly true in the case of fish!). The model allows carbon dioxide to diffuse between arterioles and the venous bed causing either a relaxation or contraction of the nearby arteriolar bed. Results show that the metabolic mechanism seems to be the dominant mechanism for cerebral autoregulation. The authors believe this to be the first time a full arterial tree algorithm has been developed to show the autoregulation mechanism. However, it is thought that the time taken for carbon dioxide to diffuse into the tissue is longer than the characteristic timescales measured for blood vessels to alter their radii in response to local brain activity. Given the small variation in radial dilation/contraction of the myogenic model which requires considerable fluid pressure acting on the stretch activated channels it is an interesting afternote to consider what possible role the myogenic mechanism could play in the autoregulation of cerebral blood flow.

Further developments by the group here at Canterbury in this particular area of modeling the autoregulation mechanism in the brain are aimed at integrating a more complex metabolic model into the vascular tree framework. This metabolic model includes a number of cellular processes which affect the calcium inside both the smooth muscle cell and the endothelial cell. From a mathematical perspective this involves the inclusion of a significant number of ordinary differential equations, particularly in modeling the calcium concentration in an associated glial cell called an "astrocyte" and the inwardly rectifying potassium channels which present themselves on the membrane of the smooth muscle cell. The astrocyte can be considered as the "bridge" from synapse to the local blood supplying vessel [37]. One end of the glial cell is located in close proximity to the post-synaptic neuron whilst the other end is firmly fixed around the vessel wall. It is thought that calcium variations cause potassium channels to open and provide "surges" of potassium into the extra-cellular space. The particular potassium channels on the blood vessel in response to these "surges" tend to hyperpolarise the smooth muscle cell thereby dilating the vessel and allow more blood to flow to the brain tissue. The mechanism of this local phenomenon is termed "functional hyperaemia" and experimental evidence tends to suggest that this is crucial in the local support of neuronal activity [38].We are therefore now able to model different cellular mechanisms in different parts of the vasculature, particularly utilising the myogenic model for the larger arteries and the more complex "astrocyte" model at the deeper levels of the vascular tree. This requires considerable compute power and as such we will utilise this model in conjunction with

distributed memory computer architectures such as the IBM Blue Gene (http://www.bluefern.canterbury.ac.nz/): mapping each part of the vasculature on to each Blue Gene node and allowing the subset of o.d.e.s which represent different cellular processes to simulate the full tree as a whole "organ".

References

1. Ursino M, Giulioni M (2003) Quantitative assessment of cerebral autoregulation from transcranial Doppler pulsatility: a computer simulation study. Med Eng Phys 25(8):655–666
2. Ursino M (1991) A mathematical-model of overall cerebral blood-flow regulation in the rat. IEEE Trans Biomed Eng 38(8):795–807
3. Olufsen MS, Nadim A, Lipsitz LA (2002) Dynamics of cerebral blood flow regulation explained using a lumped parameter model. Am J Physiol Regul Integr Comp Physiol 282(2):R611–R622
4. Moore S, David T, Chase JG, Arnold J, Fink J (2006) 3D models of blood flow in the cerebral vasculature. J Biomech 39(8):1454–1463
5. Moore S, David T (2006) Auto-regulated blood flow in the cerebral-vasculature. J Biomech Sci Eng (JSME) 1(1):1–14
6. Moore S, Moorhead K, Chase J, David T, Fink J (2005) One-dimensional and three-dimensional models of cerebrovascular flow. J Biomech Eng 127:440–449
7. Moorhead K, Doran CV, Chase JG, David T (2004) Lumped parameter and feedback control models of the auto-regulatory response in the circle of Willis. Comput Methods Biomech Biomed Eng 7(3):121–130
8. Moorhead KT, Chase JG, David T, Arnold J (2006) Metabolic model for autoregulation in the circle of Willis. J Biomech Eng 128(3):462–466
9. Moorhead K, Moore S, Chase JG, David T, Fink J (2005) Impact of decentralised control in cerebral blood flow auto-regulation using 1D and 3D models. Int J Intell Syst, Technol Appl 1(1/2):95–110
10. Ferrandez A (2001) Computational models of blood flow in the circle of Willis. PhD, University of Leeds
11. David T, Brown M, Ferrandez A (2003) Auto-regulation and blood flow in the cerebral circulation. Int J Numer Methods Fluids 43:701–713
12. Haga J, Li Y-SJ, Chien S (2007) Molecular basis of the effects of mechanical stretch on vascular smooth muscle cells. J Biomech 40:947–960
13. Harder D (1984) Pressure-dependent membrane polarisation in cat middle cerebral artery. Circ Res 55:197–202
14. Harder D (1987) Pressure induced myogenic activation of cat cerebral arteries is dependent on intact endothelium. Circ Res 60:102–107
15. Harder D, Roman R, Gebremedhin D (2000) Molecular mechanisms controlling nutrtive blood flow: role of cytochrome P450 enzymes. Acta Physiol Scand 168(4):543–549
16. Banaji M, Tachtsidis A, Delpy D, Baigent S (2005) A physiological model of cerebral blood flow control. Math Biosci 194(2):125–173
17. Gonzalez-Ferrandez J, Ermentrout B (1994) On the origin and dynamics of the vasomotion of small arteries. Math Biosci 119:127–167
18. Olufsen MS, Steele M, Taylor C (2007) Fractal network model for simulating abdominal and lower extremity blood flow during reesting and exercise conditions. Comput Methods Biomech Biomed Eng 10:39–51
19. Wiesner T, Berk B, Nerem R (1997) A mathematical model of ctosolic-free calcium response in endothelial cells to fluid shear stress. Proc Natl Acad Sci 94:3726–3731
20. Comerford A, Plank M, David T (2008) Endothelial nitric oxide synthase and calcium production in arterial geometries: an integrated fluid mechanics/cell model. J Biomech Eng 130:011010-1–011010-13
21. Dimmeler S, Fleming I, Fisslthaler B, Hermann C, Busse R, Zeiher AM (1999) Activation of nitric oxide synthase in endothelial cells by Akt-dependent phosphorylation. Nature 399:601–605
22. van Riper D, McDaniel N, Rembold C (1997) Myocin light chain kinase phosphorylation in nitrovasodilator induced swine carotid artery relaxation. Biochem Biophys Acta Mol Cell Res 1355:323–330
23. Murphy R (1980) Mechanics of vascular smooth muscle. Handbook of physiology vol II. Waverley Press, Baltimore
24. Burton A (1954) Relation of structure to function of the tissues of the wall of blood vessels. Physiol Rev 34:619
25. Edvinsson L (2002) Cerebral blood flow and metabolism. Lippincott Williams and Wilkins, Philadelphia
26. Thoman WJ, Lampotang S, Gravenstein D, van der Aa (1998) A computer model of intracranial dynamics integrated to a full-scale patient simulator. J Comput Biomed Res 31(1):32–46
27. Halsey JH, McFarland S (1974) Oxygen cycles and metabolic autoregulation. Stroke 5:219–225
28. Alastruey J, Moore S, Parker K, Peiro J, David T, Sherwin S (2007) Reduced modelling of blood flow in the cerebral circulation: coupling 1-D, 0-D and cerebral auto-regulation models. Int J Num Methods Fluids (in press)
29. Lauwers F, Cassot F, Lauwers-Cances V, Puwanarajah P, Duvernoy H (2008) Morphometry of the human cerebral cortex microcirculation: General characteristics and space-related profiles. NeuroImage 39:936–948
30. Pries A, Secomb T (2005) Microvascular blood viscosity in vivo and the endothelial surface layer. Am Heart J - Heart Cir Phys 289:H2657–H2664

31. Krogh A (1919) The number and distribution of capillaries in muscles with calculations of the oxygen pressure head necessary for supplying the tissue. J Physiol 52:409–515
32. Bloch I (1943) Some theoretical considerations concerning the interchange of metabolite between capillaries and tissue. Bull Math Biophys 5:1–14
33. Blum J (1960) Concentration profiles in and around capillaries. Am J Physiol 198(5):991–998
34. McGuire BJ, Secomb TW (2001) A theoretical model for oxygen transport in skeletal muscle under conditions of high oxygen demand. J Appl Physiol 91:2255–2265
35. Shampine LF, Reichelt MW (1997) The MATLAB ODE Suite. SIAM J Sci Comput 18:1–22
36. Lipowsky H, Zweifach B (1978) The distribution of blood rheological parameters in the microvasculature of the cat mesentary. Circ Res 43:738–749
37. Takano T, Tian GF, Peng W, Lou N, Libionka W, Han X, Nedergaard M (2006) Astrocyte-mediated control of cerebral flow. Nat Neurosci 9:260–267
38. Filosa J, Blanco V (2007) Neurovascular coupling in the mammalian brain. Exp Physiol 92:641–646